

Emission from a damped Ly α absorber at $z = 2.81$ *

P. Møller and S.J. Warren

European Southern Observatory, Karl-Schwarzschild-Straße 2, W-8046 Garching bei München, Germany

Received September 4, accepted October 31, 1992

Abstract. It is widely held that the damped Ly α absorption lines seen in the spectra of many high-redshift quasars indicate the existence of large circular slabs of gas, that shrink to form the disks of today's spiral galaxies. To attempt to detect Ly α emission from such a gas cloud, and measure its size, we have obtained a very deep image of the field of the quasar PKS0528–250 ($z_{\text{abs}} = 2.811$, $z_{\text{em}} = 2.77$) using a 23Å-wide filter centred on the damped line. From a comparison with B and V images we find three objects that are candidate sources of Ly α emission, detected at signal-to-noise ratios 13, 9, and 10. The nearest candidate lies at an angular separation of $1.6''$ from the quasar, which corresponds to a projected distance $9(5)h^{-1}\text{kpc}$, $q_0 = 0.1(0.5)$. This object is confirmed by subsequent spectroscopy to be Ly α emission from the absorber itself, on the basis of the measured velocity difference between emitter and absorber of only $50 \pm 100\text{km s}^{-1}$. The gas may be photoionised by the quasar, but we argue that hot stars are more likely the source of the ionising radiation. The line luminosity $2.5(1.1) \times 10^{42}h^{-2}\text{ergs s}^{-1}$ corresponds to a star formation rate of $2.2(1.0)h^{-2}M_{\odot}\text{yr}^{-1}$ if there is no dust. However the true value could be higher by an order of magnitude or more if dust is present. The emission-line region is possibly extended, in which case the minimum size of the absorber is $27(18)h^{-1}\text{kpc}$. The two other Ly α candidates are of similar brightness and lie within only $21''$ of the quasar. These two sources could be galaxies in a compact group. Alternatively, together with the first source, they could be regions of star formation in a single very large gas cloud, of minimum size $116(77)h^{-1}\text{kpc}$.

Key words: galaxies: formation – intergalactic medium – quasars: absorption lines – quasars: individual: PKS0528–250

1. Introduction

We know next to nothing about the sizes, morphologies, or spatial distribution of normal galaxies when the universe was young

Send offprint requests to: P. Møller

* Based on observations collected at the European Southern Observatory, La Silla, Chile.

because distant field galaxies have proven very hard to find. The redshift upper limit of the deepest magnitude-limited spectroscopic surveys $m_B < 24$ (Cowie et al. 1991; Colless et al. 1992) is close to $z = 1.0$, or a look-back time $\tau_{0.1} = 0.57$, $\tau_{0.5} = 0.65$ (where the subscripts are values of q_0). To reach much further back in time demands a different approach and one possible way to locate distant galaxies is to recognise their absorption signature in the spectra of bright high-redshift quasars. In particular if the line of sight to a distant quasar passes through the disk of a spiral galaxy, the high column density of neutral hydrogen $N_{\text{HI}} > 10^{20}\text{cm}^{-2}$ will produce a characteristic damped Ly α absorption line. One such damped absorption line is seen in the spectrum of the quasar PKS0528–250 at an absorption redshift $z_{\text{abs}} = 2.811$ ($\tau_{0.1} = 0.81$, $\tau_{0.5} = 0.87$) that is slightly higher than the quasar emission redshift $z_{\text{em}} = 2.77$ (Morton et al. 1980). We have attempted to obtain an image of the gas cloud responsible for the absorption in order to measure its size. Here we firstly summarise other attempts to find high-redshift galaxies by similar means, to put our observations in context and to explain the motivation for observing our particular target.

Wolfe et al. (1986) began a search for distant spiral galaxies by obtaining low-resolution spectra of 68 high-redshift quasars $z > 2.2$ and identifying absorption lines of large equivalent width, at wavelengths shortward of the quasar Ly α emission line. The results of subsequent high-resolution spectroscopy of this and a second sample (Lanzetta et al. 1991) confirm that many of the lines are damped, the remainder being blends of two or more absorption lines. However the number of damped Ly α lines is greater than expected, on the assumption that the comoving density and size of spiral-galaxy disks do not change with time, by a factor of at least two to four (at the 2σ level of significance and depending on q_0). One possible explanation is that spiral-galaxy disks were larger in the past. Alternatively the majority of the damped Ly α lines may be associated with some other class of object. Tyson (1988) has suggested that a population of low surface-brightness dwarf galaxies, undetected in galaxy surveys due to selection biases, could account for the discrepancy. Consequently there have been a number of attempts to obtain images of the gas clouds that give rise to the damped absorption lines.

Smith et al. (1989) tried to detect the absorbers in the light of the Ly α emission line. They obtained deep images of four

quasars (including PKS0528–250), redshifts $2.69 \leq z_{\text{em}} \leq 3.03$, through narrow-band filters centred on the central wavelength of each damped absorption line, redshifts $2.31 \leq z_{\text{abs}} \leq 2.81$. Because of the enormous optical depths over the central $\sim 20\text{\AA}$ of the absorption line the background light from the quasar is blocked out. On the other hand Ly α emission originating in the cloud can escape after multiple scatterings, if there is no significant dust. In each case the measured flux was below the 3σ detection limit, which ranged from 0.4 to $1.2 \times 10^{-16} \text{ergs cm}^{-2} \text{s}^{-1}$.

Depending on the velocity width of the emission line and provided the slit covers the emission-line region, long-slit spectroscopy may be a more efficient way of detecting the absorber. A disadvantage of the technique is that it provides the size of the absorber in only one dimension. Hunstead et al. (1990) observed the damped absorption line $z_{\text{abs}} = 2.47$ in the spectrum of the quasar Q0836+113 $z_{\text{em}} = 2.67$ at a resolution of 1.5\AA . They report the detection at the $4.0 - 4.5\sigma$ level of a faint, narrow emission line, of line flux $2.9 \times 10^{-17} \text{ergs cm}^{-2} \text{s}^{-1}$ and FWHM $< 60 \text{km s}^{-1}$. The measured line flux corresponds to a line luminosity of $3.2 \times 10^{41} h^{-2} \text{ergs s}^{-1} (q_0 = 0.5, H_0 = 100h \text{ km s}^{-1} \text{Mpc}^{-1})$. The emission is confined to the same single spatial pixel as the spectrum of the quasar, of angular size $2.2''$, which corresponds to $8.5h^{-1} \text{kpc} (q_0 = 0.5)$. Hunstead et al. argue that the close proximity of the emission-line region to the line of sight to the quasar, and its small spatial extent, support the interpretation that the absorber is a dwarf galaxy.

On the basis of subsequent spectroscopy and narrow-band imaging of the same absorber Wolfe et al. (1992) contradict this conclusion. From their spectrum (also centred on the quasar and with the slit oriented at a similar position angle to that employed by Hunstead et al.) they measure a line flux $(7.0 \pm 8.5) \times 10^{-18} \text{ergs cm}^{-2} \text{s}^{-1}$, which is consistent with zero and inconsistent with the result of Hunstead et al. In addition, from an analysis of their narrow-band images, Wolfe et al. claim to detect Ly α emission at a flux level $2.8 \times 10^{-17} \text{ergs cm}^{-2} \text{s}^{-1}$ from a galaxy centred $4''$ to the NE of the quasar, of dimensions $24 \times 11 h^{-2} \text{kpc}^2 (q_0 = 0.5)$. However this interpretation is complicated by the presence of a galaxy of redshift $z = 0.79$ at closely the same position (Lowenthal et al. 1990), and the line emission so far lacks spectroscopic confirmation.

Other observations that produced only upper limits to the Ly α emission flux from damped absorbers have been reported by Foltz et al. (1986), Deharveng et al. (1990), Pettini et al. (1990), and Lowenthal et al. (1991). To summarise, there is no case of an image of a damped Ly α galaxy detected in the light of Ly α emission for which confirmatory spectroscopy exists.

Our new observations are again narrow-band images, of total integration time 10 hours, of the quasar PKS0528–250. However, the special condition pertaining to this quasar is the possibility that the luminosity of the gas cloud in the light of Ly α will be enhanced by the proximity of the absorber to the quasar itself. Photons from the quasar shortward of the Lyman limit will photoionise the back surface of the absorber. Therefore, depending on the distance from the quasar to the absorber and the hydrogen column-density radial profile, the edge of the

cloud may be visible as a ring of Ly α emission — a silver lining. In addition, because of the declination, observations of this quasar at a dark site in the southern hemisphere, and with a narrower filter, have the potential to reach fainter flux levels than the observations of Smith et al. (1989) which were made from Lick Observatory.

Two other observations of damped absorbers bear on the problems of their size and detectability. Firstly, Briggs et al. obtained a lower limit to the size of a damped system of $8h^{-1} \text{kpc} (q_0 = 0.5)$ from observations of 21 cm absorption towards the high-redshift extended radio source PKS0458 – 020. Secondly, broad-band images taken by Steidel & Hamilton (1992) of the quasar Q0000 – 263, $z_{\text{em}} = 4.11$, show the presence of a galaxy at an angular separation of $2.8''$ from the quasar which may correspond to a damped absorption line of redshift $z = 3.39$, seen in the quasar spectrum. The galaxy is not detected in a deep broad-band exposure taken through a specially-designed U_n filter which has a long-wavelength cutoff at the Lyman limit of the damped absorber. This would be expected if the galaxy is the absorber as the flux level shortward of the galaxy Lyman limit would be low.

2. Imaging

2.1. Observations and data reduction

Our narrow-band images were obtained with the EFOSC instrument at the 3.6m telescope of the European Southern Observatory (ESO) on the nights beginning 1991 December 10 and 11. During the two nights the seeing ranged from $1.5''$ to $2.5''$, with an average value near $1.7''$. Only about one half of the second night was useful, due to intermittent clouds. The detector used was a Tektronix 512×512 CCD of pixel size $0.61''$ and readout noise $9.3e^-$. The narrow-band filter was manufactured by Omega Optical Corp. The characteristics of this filter are a central wavelength $\lambda = 4632\text{\AA}$, peak transmission $T(\lambda)_{\text{max}} = 0.52$, and FWHM 23\AA . The transmission curve is plotted in Fig. 1, together with a spectrum of the quasar. The area under the curve $\int T(\lambda) d\lambda = 12.43\text{\AA}$. In the EFOSC instrument the filter wheel is positioned in the parallel beam, inclined at an angle of 4° , which shifts the transmission curve to shorter wavelengths by 2.7\AA in the centre of the field.

Integration times for the narrow-band observations were typically 60 minutes, in which case the photon noise from the sky comfortably exceeds the readout noise. The individual frames were offset from each other by some $30''$ in a random direction, to minimise the effects of CCD defects and flat-field residuals. Eleven exposures were obtained over the two nights for a total integration time of 608 minutes. Observations were also made of spectrophotometric standard stars but could not be used because of the non-photometric conditions. Instead we have calibrated our narrow-band frames using broad-band B and V exposures as explained below.

Short exposures through broad-band B and V filters were obtained totaling eleven and eight minutes respectively. Calibration B and V exposures of the quasar and of photomet-

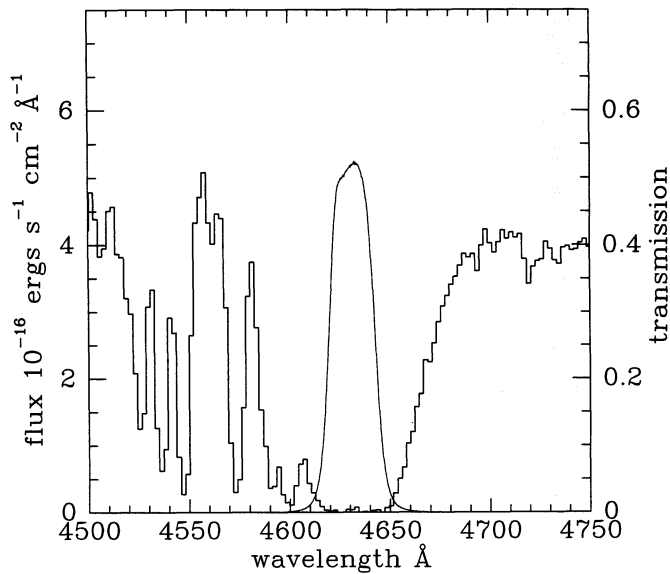


Fig. 1. Transmission curve of the narrow-band filter, and our spectrum (Sect. 3) of the quasar PKS0528–250

Table 1. Measured mean and rms sky surface brightness

passband	mean SB (mag. arcsec ⁻²)	rms SB (mag. arcsec ⁻²)
B	22.26	27.16
V	21.51	27.09
narrow	22.26	27.12

ric standard stars were obtained at the Danish 1.5m telescope on the night of 1992 February 24, when conditions were photometric. The zero point for magnitudes measured in the narrow band is on the AB system, such that for stars $m_{\text{narrow}} = -48.60 - 2.5 \log(f_{\nu})$, i.e. for objects of smooth spectral-energy distribution $m_{\text{narrow}} \equiv m_{\text{AB}}$. Alternatively a narrow emission line at wavelength λ of flux F ergs cm⁻² s⁻¹ will have a brightness $m_{\text{narrow}} = -18.00 - 2.5 \log(T(\lambda)F)$. We calibrated our narrow-band frames using stars common to the B, V, and narrow-band frames, by applying the relation $m_{\text{B}} - m_{\text{narrow}} = 0.14 + 0.40(m_{\text{B}} - m_{\text{V}})$. The colour equation was computed following the prescription of Bessell (1986) by synthesising magnitudes of the Vilnius spectrophotometric sequence (Straizys & Sviderskiene 1972) using the transmission functions for the three passbands.

From each frame dark and bias frames were subtracted, then the relative sensitivity of each pixel was corrected for by dividing by a normalised dome flat-field frame. Residual large-scale gradients in the frames were removed using exposures of the twilight sky. The frames were then registered to a common coordinate system, in all cases shifting by an integral number of pixels. (Restricting ourselves to shifts of whole pixels degrades the resolution by about 6%, but ensures that cosmic rays are not smeared out, and that pixels remain statistically independent.)

All the frames in each passband were then combined in the following manner, which is optimal for faint sources. After subtracting the sky the integrated counts in unsaturated bright stars were used to scale each frame to the same object count level. For every pixel the counts from all the frames were then averaged, weighting by the inverse of the sky variance, computed for each frame. At the same time cosmic rays were rejected using a σ -clipping algorithm. For a faint source the detected photons from the object make a negligible contribution to the noise, and the noise in each pixel is the same as the noise in a sky pixel. For this reason the procedure described above maximises the signal-to-noise ratio (S/N) of faint objects.

2.2. Results

The final B and narrow-band images are reproduced in Figs. 2a and b, which show a region 320×408 pixels ($194'' \times 248''$) surrounding the quasar marked Q . The measured brightness of the quasar is $m_{\text{B}} = 18.52$, $m_{\text{V}} = 17.72$. Details of the sky brightness and the noise in the sky are provided in Table 1. There are a number of bright stars in the field and these produce problematic ghost images in the narrow-band frame, caused by multiple internal reflections in the filter. These appear as a series of blobs emanating from each star in the SW direction, diminishing rapidly in intensity with each reflection and becoming more elongated. For example the primary ghost image is visible in the case of the star marked A in Fig. 2b. The intensity of the primary ghost image relative to the star is 0.5%. The star marked B is the brightest of a pair, and here the primary ghost is not seen because of the chosen intensity scaling. The rod-like feature visible to the SW is the secondary ghost image, of intensity 0.02% relative to the star, while the higher-order ghost images merge to form a very faint extended jet which is just visible in the figure.

Regrettably the sought-for shining doughnut is not seen. However in the narrow-band frame near the position of the quasar there is a slightly elongated image. Whereas some light from the quasar will be transmitted by the filter (Fig. 1) the measured position of this image does not coincide exactly with the position of the quasar. A close-up view of the two frames is presented in Figs. 3a and b, where the centroid of the quasar image, measured in the B frame, is marked by a small cross (note that Fig. 3a has been smoothed). From Fig. 3b it is clearly seen that not all of the narrow-band emission is centered on the quasar, and we conclude that the image in the narrow-band frame is the sum of a contribution from the quasar and light from an additional faint object located a short distance to the SE of the quasar. This source is plausibly the absorber, and is named here S1.

To establish the contribution of the quasar to the measured flux we considered firstly multiplying a flux-calibrated spectrum of the quasar by the filter transmission curve. However the filter was measured in a converging beam, so the curve is the average of the transmission curves for each light ray, and these individual curves are shifted in wavelength by a different amount depending on the angle of incidence. Shifting the

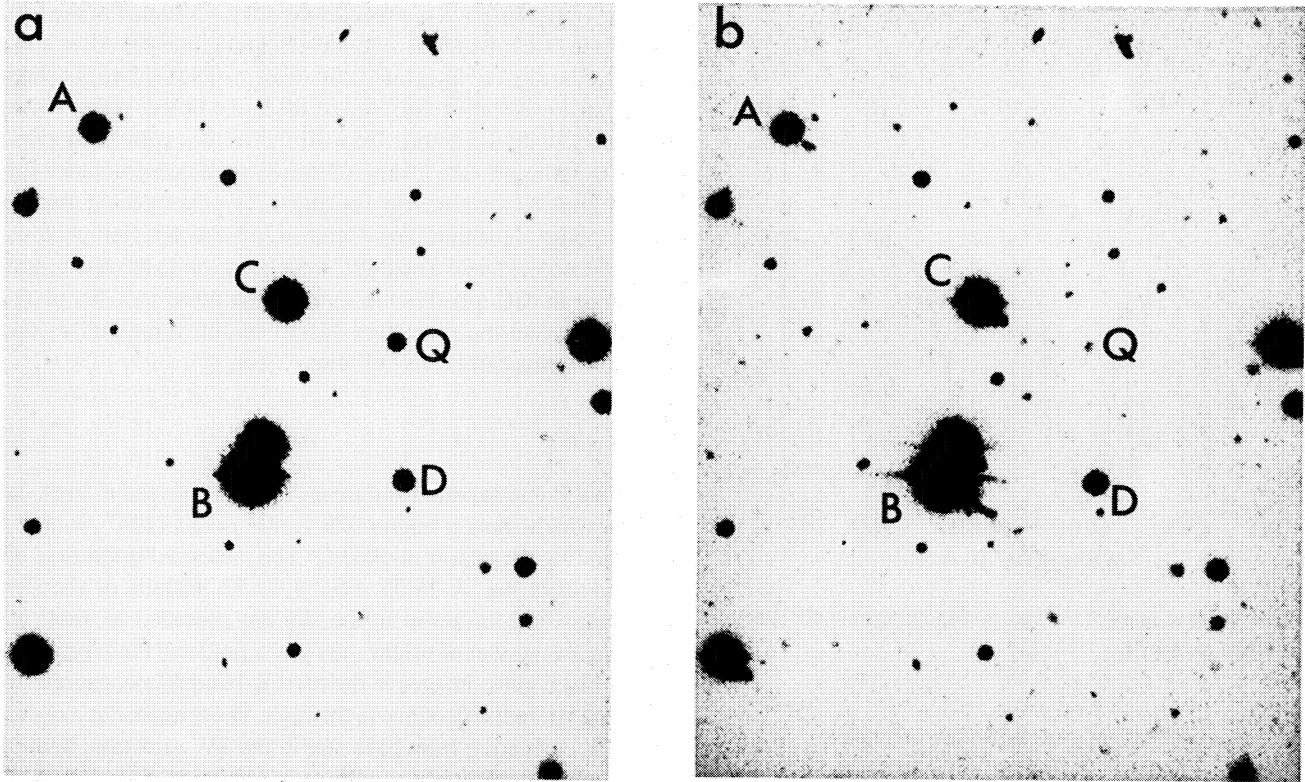


Fig. 2. The region 320×408 pixels ($194'' \times 248''$) surrounding the quasar. N is up and E is to the left. (a) combined B frame, (b) combined narrow-band frame. Note that the quasar PKS0528–250, marked Q, is almost invisible in the narrow-band frame. The primary ghost is visible to the SW of star A, the secondary and tertiary to the SW of the star pair marked B. Other stars mentioned in the text are marked C and D

transmission curve by as little as $\sim 1 \text{ \AA}$ results in an appreciable difference in the transmitted flux. We could not therefore establish the correct transmission curve, for parallel light, to the required wavelength accuracy. Instead we decided to obtain an estimate of the maximum amount of flux in the narrow-band frame which could possibly be due to the quasar. We proceeded by analysing the narrow-band frame using the photometry package DAOPHOT (Stetson 1991). DAOPHOT employs simultaneous multiple-profile fitting to blended objects, using a point spread function (PSF) constructed by averaging the profiles of a number of bright unsaturated stars in the frame. The result for the image in question was that an acceptable fit was obtained with two point sources. One source, containing 52% of the flux, was found by DAOPHOT to lie at a position which coincides with the position of the quasar as determined in the broad-band frames, the offsets being 0.15 ± 0.26 and 0.19 ± 0.26 pixels in the EW and NS directions respectively. We have assumed, for the present, that this represents the leaked light, and we have subtracted this source from the frame. This is a conservative assumption since some of the light at the position of the quasar could be emitted by the absorber, so the remaining 48% of the flux is a *lower limit* to the flux of S1. The decomposition into two sources was, however, vindicated by our follow-up spectroscopy (Sect. 3.2).

The remaining object, the source S1, is detected at a S/N of 13. A scaled PSF was also subtracted at the position of the star

marked C as there is a source contaminated by the secondary ghost image of this star. In this case we constructed the PSF using the star pair marked B, as they are the only stars bright enough to establish the form of the PSF at large radii. Because these two stars and star C are saturated the subtraction is incorrect near the centre of the star. The resulting frame is shown in Fig. 3c. A smoothed version of this frame was formed by convolution with a Gaussian profile, of σ one pixel, and is shown in Fig. 3d.

Any galaxy at a redshift near $z = 2.81$ with a strong Ly α emission line will appear bright in the narrow-band frame relative to the B and V frames. To search the frames for candidate Ly α emitters, in addition to S1, we used the FOCAS software package (Valdes 1982) to measure positions and magnitudes for stars and galaxies in the (full) B, V, and narrow-band frames. This resulted in a catalogue of magnitudes and colours for 71 objects detected in the narrow band frame at $S/N > 6$. The corresponding two-colour diagram is shown in Fig. 4. The FOCAS software proceeds by convolving the frame with a detection filter: groups of connected pixels above a threshold isophote in the smoothed frame define object apertures, which are applied to the unsmoothed data to measure pseudo-isophotal magnitudes. When an object was detected in the narrow-band frame but not in one of the broad-band frames we integrated the broad-band flux inside the registered narrow-band aperture. Because these few objects are very faint in the broad-band frames the errors on the colours are large. We applied a small correction to the FOCAS

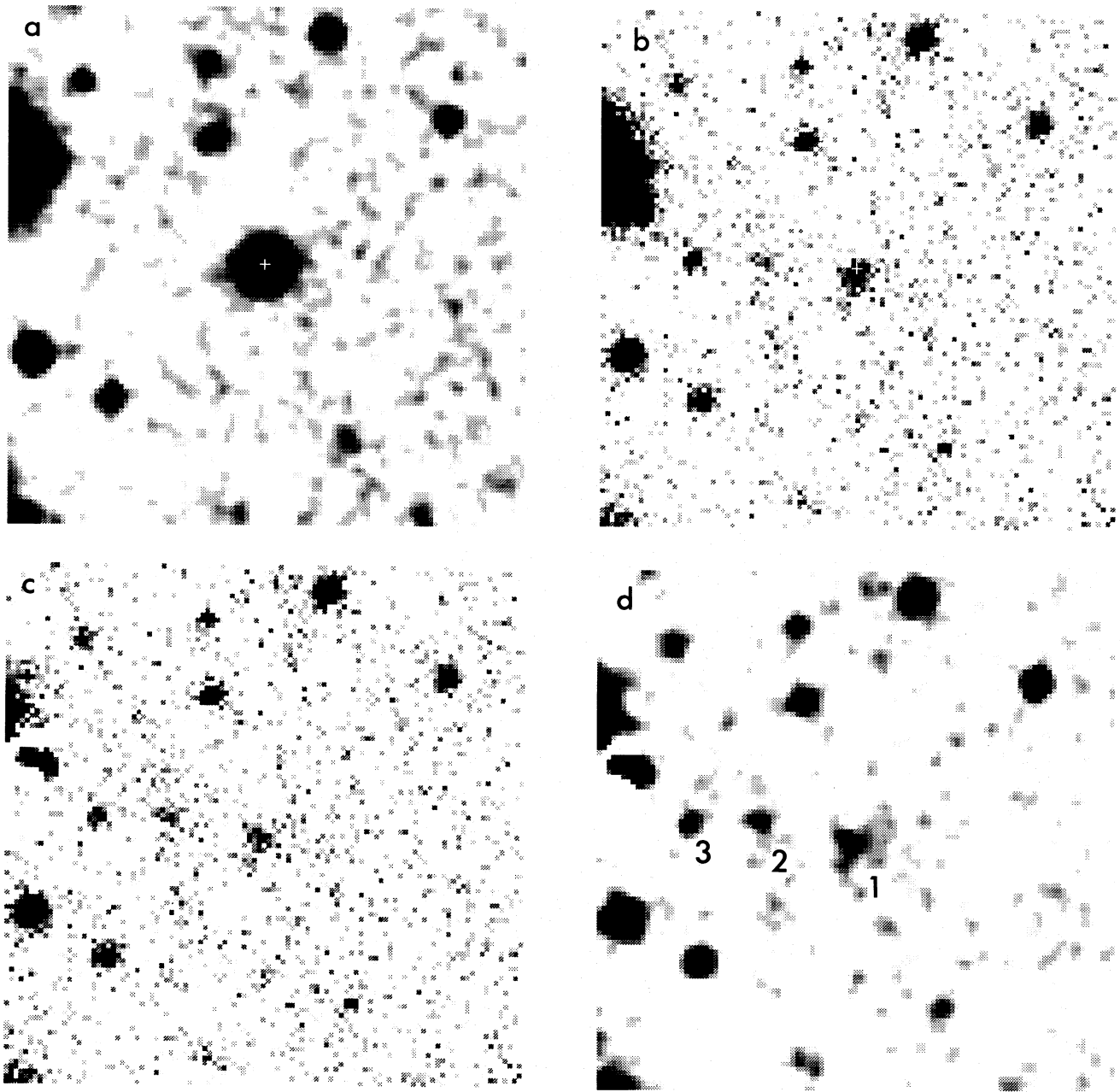


Fig. 3. Expanded view of the region 107×107 pixels ($65'' \times 65''$) surrounding the quasar. N is up and E is to the left. (a) combined B frame smoothed by convolution with a Gaussian profile of σ one pixel, (b) combined narrow-band frame, (c) narrow-band frame with contribution from the quasar, and the ghost image to the SW of star C removed, (the reason for the poor subtraction at the centre of the star is given in the text), (d) is frame (c) smoothed with a Gaussian of σ one pixel. The centroid of the quasar image is marked by a small cross in (a) and (b)

magnitudes (of order 0.01 mag. in each band) by computing the average offset between the FOCAS isophotal magnitudes and the total magnitudes of a number of bright unsaturated stars measured by DAOPHOT. Thus for bright objects the final magnitudes are total magnitudes, whereas for faint objects light is lost outside the FOCAS isophote.

To measure the broad-band magnitudes of S1 it is necessary to subtract the quasar image from the B and V frames. However we found that, given the seeing conditions, the source lies too close to the position of the quasar to achieve this to the accuracy

required. Therefore we cannot quote useful estimates of the broad-band B and V magnitudes of S1, but this will be possible with deeper images obtained in better seeing conditions.

An object with an emission line in the narrow passband will lie in the lower left corner of Fig. 4; conversely any object with Ly α absorption at $z_{\text{abs}} = 2.81$ will lie in the upper right-hand part. The quasar is the source in the far upper right. In the lower left corner there are two sources with colours $m_{\text{narrow}} - m_{\text{V}} < -2$, $m_{\text{B}} - m_{\text{narrow}} > 2$, which are therefore excellent emission line candidates. Furthermore both objects lie in the

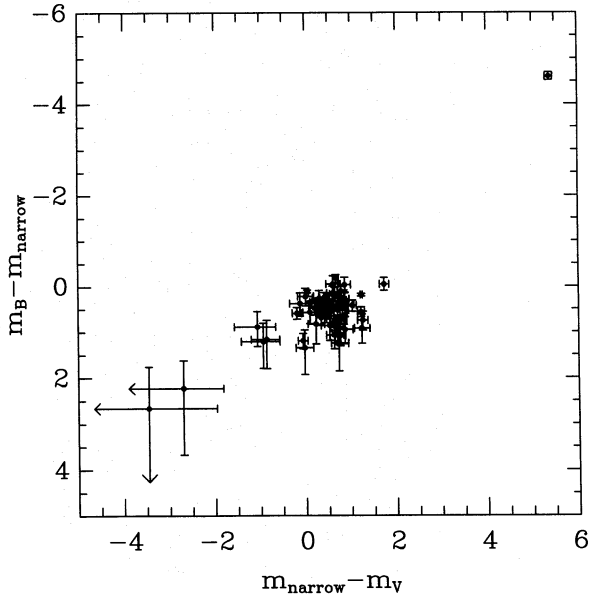


Fig. 4. Two-colour diagram of 71 stars and galaxies detected at $S/N > 6$ in the narrow-band frame. The quasar lies in the upper right-hand corner of the plot. The two objects in the lower left-hand corner are the sources S2 and S3, and are candidate Ly α emitters at $z = 2.81$. The source S1 does not appear in this plot as we are unable to determine reliably the broad-band magnitudes of this object

Table 2. Candidate Ly α emitters $z = 2.81$: Positions

source	Pos. offset from quasar (arcsec.)		Proj. distance (kpc)		FWHM $1 - \sigma$ range (arcsec)
	$q_0 = 0.1$	$q_0 = 0.5$	$q_0 = 0.1$	$q_0 = 0.5$	
S1	0.46E	1.58S	$9.2h^{-1}$	$6.1h^{-1}$	$1.3^{+0.5}_{-0.5}$
S2	11.79E	0.93N	$66.4h^{-1}$	$44.0h^{-1}$	$0.0^{+1.2}_{-0.0}$
S3	20.66E	0.81N	$116.2h^{-1}$	$76.9h^{-1}$	$1.4^{+0.4}_{-0.4}$

vicinity of the quasar, at distances of $12''$ and $21''$. We have named these sources S2 and S3, and their locations are indicated in Fig. 3d. The positions of the three candidate Ly α emitters are summarised in Table 2. The quoted offsets assume that the Y axis of the CCD was accurately aligned N-S. For spectroscopy accurate orientation of the slit may be achieved by reference to the position of star D (Fig. 2a). The position angle (PA) of the line joining the quasar and star D is 183.3° (PA measured N through E).

To obtain limits to the size of the sources S1,2,3 we have fitted a circular Gaussian function to a region 11×11 pixels centred on each object. We have corrected the 1σ limits to the FWHM for the contribution of the seeing, to provide 1σ limits to the intrinsic FWHM, which are quoted in Table 2. The rather weak constraints reflect the mediocre seeing conditions. There is a faint object lying $3''$ SSE of S1 (Fig. 3d), of brightness $m_{\text{narrow}} = 24.9 \pm 0.2$, which may be an extension of S1, but for the moment is considered as a separate object. In addition there

is possibly some diffuse emission in the vicinity of S1. Deeper imaging will be needed to confirm its reality.

The brightnesses and inferred line fluxes of the three candidates are provided in Table 3. The line fluxes were calculated assuming $T(\lambda) = 0.5$. There are three other sources plotted in Fig. 4 that are relatively bright in the narrow-band frame. These objects lie in widely separated locations around the frame. We intend to obtain deeper images in B and V to verify their colours. In addition one object, besides the quasar, is indicated to have strong absorption, and merits further attention.

We can compare the depth reached in our narrow-band image with the depth of the observations of the same quasar by Smith et al. (1989). The measured noise in the sky in our frame corresponds to a line flux $1.8 \times 10^{-18} \text{ ergs cm}^{-2} \text{ s}^{-1} \text{ arcsec}^{-2}$ (for a line of wavelength near the centre of the filter), which is a factor six lower than the noise in their image. Our three candidate Ly α emitters are detected at signal-to-noise ratios of 13, 9 and 10 in our image, so it is not surprising that they were not detected in the Lick observations.

To summarise the imaging observations, we have detected three sources in the vicinity of the quasar that appear to have emission lines at a wavelength near $\lambda = 4632\text{\AA}$, and may be galaxies at a redshift $z = 2.81$. One source, S1, would lie at a projected separation of less than $10h^{-1} \text{ kpc}$ from the quasar (Table 2) and may be the absorber itself. In the next section we present the results of spectroscopic observations of this source.

3. Spectroscopy

3.1. Observations and data reduction

Spectra of the source S1 were obtained with the EMMI instrument at the New Technology Telescope, ESO, on the nights beginning 1992 February 4 and February 25.

For the observations of February 4 the blue arm of EMMI was used with a $2''$ wide slit at position angle 159.3° , and a grating of 600 grooves mm^{-1} blazed at 3500\AA . The wavelength coverage was $4110 < \lambda < 5040\text{\AA}$. For this combination the nominal resolution at $\lambda = 4630\text{\AA}$ is 4.7\AA . However because the seeing averaged $1.2''$ the true resolution can be better if the transverse angular size of the source is less than the slit width. In fact for a point source the resolution is set by the sampling. The detector was a Tektronix 1024×1024 CCD, binned by a factor two in the dispersion direction, giving a pixel size $0.36'' \times 1.8\text{\AA}$. The total integration time was 180 minutes, split equally between three exposures. These data are of inferior quality, due to problems associated with the CCD readout electronics. Each frame exhibits a different complex wavy noise pattern, as well as a large number of sharp spikes (in addition to cosmic rays) and holes that have the same origin in the readout of the CCD. The Fourier components of the wavy patterns are recognisable in the power spectrum of each frame, and were removed by filtering. Even so the measured readout noise in the filtered frames was $20e^-$, which greatly exceeds the nominal value.

For the observations of February 25 we used the red arm of EMMI with a $2''$ wide slit at position angle 155.1° , and a

Table 3. Candidate Ly α emitters $z = 2.81$: Photometry.

source	m_{narrow}	flux (ergs cm $^{-2}$ s $^{-1}$)	luminosity (ergs s $^{-1}$)		SFR (M $_{\odot}$ yr $^{-1}$)	
			$q_0 = 0.1$	$q_0 = 0.5$	$q_0 = 0.1$	$q_0 = 0.5$
S1	23.08	$(7.4 \pm 0.6) \times 10^{-17}$	$2.5 \times 10^{42} h^{-2}$	$1.1 \times 10^{42} h^{-2}$	$2.2 h^{-2}$	$1.0 h^{-2}$
S2	23.69	$(4.2 \pm 0.5) \times 10^{-17}$	$1.4 \times 10^{42} h^{-2}$	$6.2 \times 10^{41} h^{-2}$	$1.3 h^{-2}$	$0.6 h^{-2}$
S3	23.44	$(5.3 \pm 0.5) \times 10^{-17}$	$1.8 \times 10^{42} h^{-2}$	$7.9 \times 10^{41} h^{-2}$	$1.6 h^{-2}$	$0.7 h^{-2}$

Note that for sources S2 and S3 the assumed redshift $z=2.81$ remains to be confirmed by spectroscopy

grism of 600 grooves mm $^{-1}$ blazed at 5300Å. The wavelength coverage was $4190 < \lambda < 6400$ Å. The nominal resolution for this combination is 8.4Å. The seeing averaged 0.9'' so, as before, for a point source the resolution was set by the sampling. The detector was a Thomson 1024 \times 1024 CCD, of pixel size $0.44'' \times 2.2$ Å, and readout noise $5.3e^-$. The total integration time was 83 minutes, split between two exposures. Relative to the blue arm the total throughput for this configuration at $\lambda = 4630$ Å is lower by a factor 2, largely due to the lower quantum efficiency of the CCD. However, because of the lower readout noise the red spectra are sky noise dominated, and hence the S/N for a faint source will be similar for a given integration time.

The first stage of the data reduction was the subtraction of dark and bias frames. After this the majority of cosmic rays and other sharp positive spikes were identified, by comparing frames, and removed by fitting a two-dimensional surface to surrounding pixels and interpolating. The blue-arm frames were Fourier filtered at this stage. All frames were then corrected for pixel sensitivity variations, and the sky was subtracted. The three blue-arm and two red-arm frames were then calibrated onto a linear wavelength scale, pixel size 2.16Å, using transformations derived from Helium-Argon spectra. The rms errors in the line fits were 0.2Å, except redward of 5700Å in the red-arm data, where there were no usable lines. As pointed out above, the seeing FWHM was smaller than the slit-width, and this results in a higher resolution than nominal but also in an uncertainty in the zero point of the wavelength calibration, if the object was not placed precisely in the centre of the slit. This was corrected for as described below. The spectroscopic frames were combined in the same way as the image frames, with weights that maximise the S/N for faint sources. Firstly individual sums of the three blue frames and two red frames were formed, to allow a comparison of the results from the two nights. The summed red frame was then rebinned to the same spatial pixel size as the summed blue frame, and the two were combined, again with optimal weights.

One dimensional spectra of the quasar were extracted from each image using a variance-weighting algorithm which maximises the S/N of the extracted spectrum. The individual spectra were then combined into red and blue summed 1-D spectra. The spectra were flux calibrated onto a relative scale, through observations of the standard star L970-30 (Oke 1974), and subsequently corrected to an absolute scale using the measured V magnitude. The required shift was 0.23 mag. Since we used a

flux conserving extraction algorithm, this calibration also applies to the 2-D frame.

To quantify any zero-point error in the wavelength calibration, due to the slit width, we measured the absorption lines in our spectra, and searched the literature for line lists obtained from high resolution, high S/N data. Comparing our line wavelengths against those of Chen & Morton (1984) and Sargent et al. (1988) we found offsets of 1.1Å and 2.1Å for the blue and the red frames respectively. These corrections correspond to a miscentering of about 0.4'' in both cases.

3.2. Results

In the final spectroscopic frame, Fig. 5, a faint patch of emission is visible at the central wavelength of the damped absorption line, offset spatially a small distance from the centerline of the quasar. The significance of the emission line is 4.2σ . The fluxes measured in the summed blue and red frames are consistent with each other, and the fluxes measured in each of the five frames lie within 1σ of that measured in the combined frame. The measured position and flux of the line, provided below, agree with the values found from the imaging, and leave no doubt that we have detected the source S1.

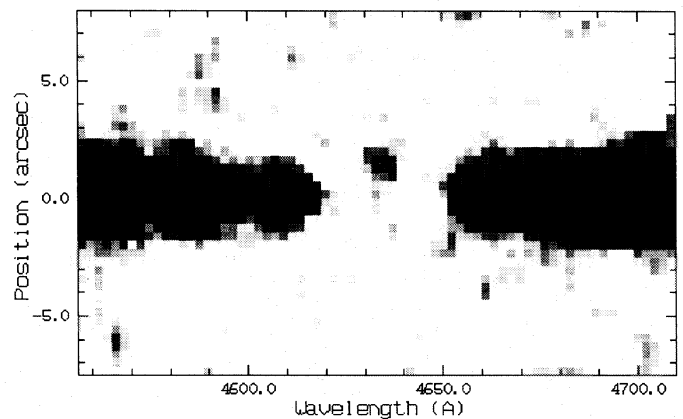


Fig. 5. Two-dimensional spectroscopic frame, smoothed by convolution with a Gaussian profile of σ one pixel. The dark band is the spectrum of the quasar, and the prominent gap is the damped absorption line. The emission line from the source S1, detected at the 4.2σ level, lies just above the absorption trough, at an angular separation of $1.32''$ from the quasar

The flux in the line, measured in a 6-pixel circular aperture, is $(6.9 \pm 1.6) \times 10^{-17} \text{ ergs cm}^{-2} \text{ s}^{-1}$, which is in good agreement with the value measured from our narrow-band frames. This suggests that the assumption followed in subtracting the quasar light from the narrow-band frame (Sect. 2) was correct, and that we have captured most of the light from the source through the $2''$ slit. The other properties of the emission line were measured by fitting an elliptical Gaussian profile, PA = 0° , to the region 9×9 pixels centred on the emission line. The measured distance from the quasar is $1.32 \pm 0.13''$, and is in agreement with the position of the source measured in the image frame, $1.65 \pm 0.15''$. In the spatial direction we found a value for the FWHM of the source, after correction for seeing, of $0.0''^{+0.7}_{-0.0}$. This estimate does not conflict with the result obtained from the narrow-band image, but again the range is not strongly constrained, this time due to the poor S/N. The faint source adjacent to S1 seen in the narrow-band frame is not detected in the spectroscopic frame, but this is not surprising as it is a factor of five fainter. We cannot therefore tell at this time whether the extension is also line emission. In the wavelength direction we measured a central wavelength of $4634.3 \pm 1.2 \text{ \AA}$, which corresponds to a redshift $z_{\text{em}} = 2.8121 \pm 0.0010$ for Ly α . Referring to the above discussion on the wavelength calibration, since we do not know whether the source covers the slit in the transverse direction, the quoted error in the wavelength, 80 km s^{-1} , includes an allowance for this additional source of uncertainty. The measured FWHM of the line, uncorrected for the resolution, is $6.1^{+1.8}_{-1.6} \text{ \AA}$. Again, we cannot correct properly for the instrument resolution, but assuming a value $\sim 4 \text{ \AA}$ (as is appropriate for a point source) we obtain an estimate of the FWHM of the line of $300^{+140}_{-170} \text{ km s}^{-1}$.

3.3. Redshift and H I column density of the absorber

A typical damped Ly α absorber is characterised by the presence of many absorption lines from low ionisation species. These lines will at high resolution usually reveal a complex multi-component structure of many clouds with a total velocity spread of $2 - 300 \text{ km s}^{-1}$, and it is not clear whether the large H I column density belongs to just one of these clouds or is distributed between them. Accordingly there is some uncertainty in using those strongly saturated metal lines to determine the redshift of the absorber. However the determination of the redshift and column density of the damped Ly α absorption line itself is complicated by the fact that it is absorbing on top of the Ly α and NV emission lines of the background quasar. Morton et al. (1980) found $z_{\text{abs}} = 2.81100$ and $\log(N_{\text{HI}}) = 21.27 \pm 0.08$, while Foltz et al. (1988) from their higher resolution but lower S/N spectrum found $z_{\text{abs}} = 2.8110 \pm 0.0003$ and $\log(N_{\text{HI}}) = 21.1 \pm 0.3$. It appears that in neither case was the effect of the emission lines allowed for in the fitting. For this reason we have made a new estimate of the redshift and column density of the damped system, using a model quasar spectrum designed to approximate the unabsorbed spectrum, and fitting the absorbed model spectrum to the data. The model comprises a power-law continuum and emission lines of equivalent width (EW) ratios

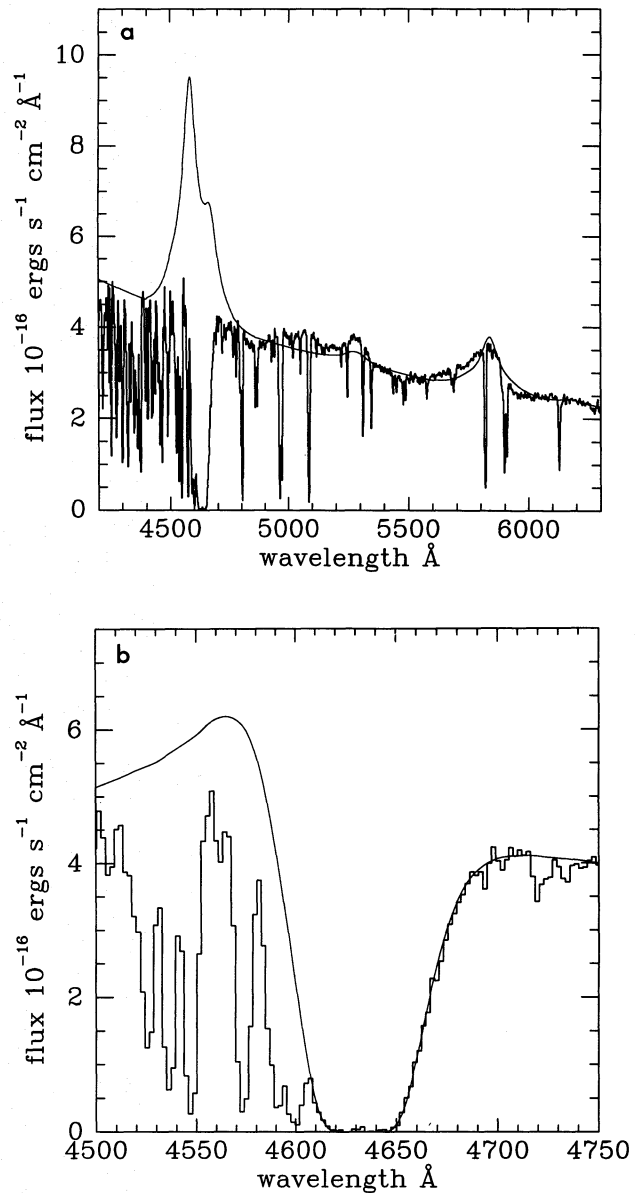


Fig. 6. (a) model quasar spectrum before absorption, and actual spectrum, (b) comparison of absorbed model spectrum with the quasar spectrum, for best-fit values of the redshift and column density of the damped system

that are typical for quasars, with the EWs scaled to the measured value for the CIV line. The line profile model is that of Boyle (1990). Values for the emission redshift of the quasar in the range $2.765 < z_{\text{em}} < 2.779$ have been reported, and we have assumed $z_{\text{em}} = 2.77$, but the results are not very sensitive to this choice. In Fig. 6a we show our model spectrum overlain on the spectrum of the quasar. Our spectrum of S1 was obtained with the slit aligned to include the quasar as well, so the final quasar spectrum is the result of over four hours integration. The S/N of the spectrum in the continuum is ~ 80 so even though it has only moderate resolution it is well suited for fitting the damped Ly α line. In Fig. 6b we show our best fit to

the damped Ly α line, for which the redshift and column density are $z_{\text{abs}} = 2.8115 \pm 0.0007$, $\log(N_{\text{HI}}) = 21.35 \pm 0.01$. Because of the resolution of our spectrum it is not surprising that shortward of $\lambda \sim 4600\text{\AA}$ the model lies above the highest points in the quasar spectrum, because of the presence of unresolved Ly α -forest absorption lines.

A further clue to the redshift of the absorber comes from the detection of absorption lines of NiII. Meyer & York (1987) reported the identification of the NiII lines of restframe wavelength $\lambda = 1709.6, 1741.5\text{\AA}$ at a redshift of $z_{\text{abs}} = 2.8112 \pm 0.0003$. We confirm their detection of NiII in this system through the identification in our spectrum of two other NiII lines, of restframe wavelengths $\lambda 1317.2, 1370.1\text{\AA}$. This is the only quasar absorption system in which NiII lines have so far been detected, and it appears indisputable that these lines are tracers of high HI column density.

To sum up our measurements of the redshifts we find $z_{\text{em}} = 2.8121 \pm 0.0010$ and $z_{\text{abs}} = 2.8115 \pm 0.0007$. The redshift difference is $\Delta z = 0.0006 \pm 0.0012$, or in terms of velocity $\Delta v = 50 \pm 100\text{km s}^{-1}$. The measured velocity difference between emitter and absorber is smaller than the error, and we therefore conclude that we have detected Ly α emission from the absorbing cloud.

4. Discussion

Before drawing further conclusions on the nature of the source S1, the difference between the redshift of the damped absorption line, $z_{\text{abs}} = 2.8115$, and the quasar emission redshift, $z_{\text{em}} = 2.77$, deserves comment. The apparent velocity of the cloud towards the quasar of $\Delta v = 3300\text{km s}^{-1}$ is remarkably high, but this is probably an overestimate of the true relative velocity. Corbin (1992) and Espey et al. (1992) have found that the high ionisation lines in quasar spectra are typically shifted to the blue by many hundred km s^{-1} relative to the true quasar redshift (established from the low-ionisation lines). Seemingly the shift of the CIV emission line is correlated with the reciprocal of the restframe EW, although there is a large scatter around the trend. Because of the scatter we cannot establish the true redshift of the quasar accurately. Nevertheless, the absorption-corrected CIV restframe EW of $\sim 15\text{\AA}$ suggests a shift $\sim 1500\text{km s}^{-1}$. Therefore a value for the true velocity difference between absorber and quasar $\Delta v \sim 2000\text{km s}^{-1}$ (or less) is quite likely, and it is plausible to associate the quasar and the absorber with two galaxies in a cluster, that is probably quite rich.

We cannot for the moment easily distinguish between the alternatives that the Ly α emission is due to star formation or to photoionisation by the quasar. One argument in favour of the latter is the fact that the detected flux is relatively strong when compared to the quoted upper limits, or possible detections, in the deepest previous searches. In the case of three quasars PHL 957 (Lowenthal et al. 1991), Q1337+113 (Smith et al. 1989), and Q0836+113 (Hunstead et al. 1990; Wolfe et al. 1992) searches have been made which would have detected an emission-line object of flux similar to that reported here, or in some cases a factor of two fainter (in the case of PHL 957, where spectroscopy

was used, supposing the object to lie within $2''$ of the quasar, we estimate an 80% chance of detection). The two reported detected objects in the case of Q0836+113 are both more than a factor of two fainter than S1, and in any case their reality is open to doubt (see Sect. 1). We must conclude that at these redshifts $z \sim 2.5$ a typical damped Ly α absorber is fainter in Ly α emission than S1. The detection of an unusually strong emitter searched for under the hypothesis that its emission would be enhanced by the presence of the quasar clearly supports that hypothesis. However the morphology of the emitter apparently does not. We had hoped to detect the absorber in silhouette. In this case the visibility of the outline is dependent on the relative positions of the quasar, absorber, and observer, and the gas-density profile in the cloud, so one cannot generalise much on the expected morphology of the visible line-emitting region. As a rule though, if one does not see the whole outline one might expect to see a partial ring, or crescent, and the emission-line region would probably be extended in a direction perpendicular to the line joining S1 and the quasar. As this does not appear to be the case this is an argument in favour that star formation is the source of ionising radiation, and on balance we consider this the more likely explanation. All the same, given the mediocre seeing, the ring might still exist but be rather thin, so a deeper image taken under better seeing conditions is desirable. With a high S/N spectrum the line profile might be used to distinguish between the two processes. If the Ly α radiation originates deep within the cloud, as might be the case if the observed line is due to star formation, the observed line may possess a double-horned profile (Urbaniak & Wolfe 1981).

From our provisional interpretation of S1 as a region of star formation, follows the prediction that future deeper searches around damped Ly α absorbers should detect Ly α emission at flux levels which are within the reach of current instrumentation. If new deeper searches fail to confirm that prediction, we would have to revise our interpretation.

We now consider whether our present results help to resolve the issue of whether the damped lines are associated with dwarf galaxies (Hunstead et al. 1990) or extended spiral-galaxy disks (Wolfe et al. 1986). The pertinent properties of the source S1 are provided in Tables 2 and 3. The projected distance from the centre of the source to the quasar (Table 2) provides a lower limit to the size of the absorber, but this is not so large as to eliminate the dwarf-galaxy hypothesis. However, as mentioned in Sect. 2, the source S1 probably has an extension in the SSE direction. The projected distance from the quasar to the centre of this tail is $26.6h^{-1}\text{kpc}(q_0 = 0.1)$, $17.6h^{-1}\text{kpc}(q_0 = 0.5)$. If the tail is confirmed by deeper spectroscopy this large minimum size would support the interpretation of Wolfe et al. (1986).

It is quite surprising that the two other best candidate Ly α emitters, in the whole frame, lie within an angular distance of only $21''$. If subsequent spectroscopy confirms emission lines in these objects, their close proximity to each other suggests either that they form a compact group of galaxies, or that they are individual regions of star formation in a single very large galaxy or proto-galaxy, of dimension $\sim 100\text{kpc}$ (Table 2). Since the narrow-band filter has a width of several hundred km s^{-1} ,

the measurement of redshifts very similar to that of S1 would support the latter suggestion.

The line luminosities of the three sources (assuming that S2 and S3 lie at $z = 2.81$) are provided in Table 3. Also provided are the star formation rates computed from the H α line flux using the expression derived by Kennicutt (1983), and assuming a Ly α /H α flux ratio of 10 and negligible dust extinction. As is well known even small quantities of dust can greatly reduce the Ly α line flux, as resonant scattering of the Ly α photons increases the escape path length enormously, and hence the absorption. Even for a dust to gas ratio one-tenth the value in the local interstellar medium, the attenuation can be an order of magnitude or more for such a high-column density damped system as that observed here (Charlot & Fall 1991). The attenuation depends on the column density of neutral hydrogen N_{\perp} along the shortest escape path for the Ly α photons, which could lie within a large range. If subsequent spectroscopy reveals the double-horned profile of the Ly α line it will be possible to estimate N_{\perp} from the splitting width (Urbaniak & Wolfe 1981). Meanwhile the star formation rates quoted are only lower limits.

Acknowledgements. We thank especially Massimo Della Valle who obtained the blue-arm spectra for us, and Helge Jønch-Sørensen who donated photometric time on the 1.5m Danish Telescope for calibration images. We are grateful to Peter Shaver and James Lowenthal for many useful comments on the manuscript. The technique for removing the noise pattern in our blue-arm spectroscopic frames was suggested by Chris Haniff.

References

- Bessell, M. S. 1986, PASP, 98, 1303
 Boyle, B.J. 1990, MNRAS, 243, 231
 Briggs, F.H., Wolfe, A.M., Liszt, H.S., Davis, M.M., Turner, K.L. 1989, ApJ, 341, 650
 Charlot, S., Fall, S.M. 1991, ApJ, 378, 471
 Chen, J., Morton, D.C. 1984, MNRAS, 208, 167
 Colless, M., Ellis, R.S., Broadhurst, T.J., Taylor, K., Peterson, B.A. 1992, preprint
 Corbin, M.R. 1990, ApJ, 357, 346
 Cowie, L.L., Songaila, A., Hu, E.M. 1991, Nat, 354, 460
 Deharveng, J.M., Buat, V., Bowyer, S. 1990, A&A, 236, 351
 Espey, B.R., Carswell, R.F., Bailey, J.A., Smith, M.G., Ward, M.J. 1989, ApJ, 342, 666
 Foltz, C.B., Chaffee, F.H., Weymann, R.J. 1986, AJ, 92, 247
 Hunstead, R.W., Pettini, M., Fletcher, A.B. 1990, ApJ, 356, 23
 Foltz, C.B., Chaffee, F.H., Black, J.H. 1988, ApJ, 324, 267
 Kennicutt, R.C. 1983, ApJ, 272, 54
 Lanzetta, K.M., Wolfe, A.M., Turnshek, D.A., Lu, L., McMahon, R.G., Hazard, C. 1991, ApJS, 77, 1
 Lowenthal, J., Caulet, A., Green, R.F., Hogan, C.J., Brown, L.W., Oliverson, R.J., Woodgate, B.E. 1990, BAAS, 22, 805
 Lowenthal, J.D., Hogan, C.J., Green, R.F., Caulet, A., Woodgate, B.E., Brown, L., Foltz, C.B. 1991, ApJ, 377, L73
 Meyer, D.M., York, D.G. 1987, ApJ, 319, L45
 Morton, D.C., Chen, J., Wright, A.E., Peterson, B.A., Jauncey, D.L. 1980 MNRAS, 193, 399
 Oke, J.B. 1974, ApJS, 42, 333
 Pettini, M., Boksenberg, A., Hunstead, R.W. 1990, ApJ, 348, 48
 Smith, H.E., Cohen, R.D., Burns, J.E., Moore, D.J., Uchida, B.A. 1989, ApJ, 347, 87
 Sargent, W.A.W., Boksenberg, A., Steidel, C.C. 1988, ApJS, 68, 539
 Steidel, C.C., Hamilton, D. 1992, AJ, 104, 941
 Stetson, P. 1991, "DAOPHOT II Users' Manual" (ESO)
 Straižys, V., Sviderskiene, Z. 1972, Bull. Vilnius Astr. Obs., 35
 Tyson, N.D. 1988, ApJ, 329, L57
 Urbaniak, J.J., Wolfe, A.M. 1981, ApJ, 244, 406
 Valdes, F. 1982, "FOCAS Users' Manual" (Tucson:NOAO)
 Wolfe, A.M., Turnshek, D.A., Smith, H.E., Cohen, R.D. 1986, ApJS, 61, 249
 Wolfe, A.M., Turnshek, D.A., Lanzetta, K.M., Oke, J.B. 1992, ApJ, 385, 151

This article was processed by the author using Springer-Verlag L^AT_EX A&A style file version 3.